Contents lists available at ScienceDirect

Arabian Journal of Chemistry

journal homepage: www.ksu.edu.sa

Original article

The enhanced adsorption of layered double hydroxides modification from single to ternary metal for fluoride by TEA-assisted hydrothermal method

Tian Huiyuan [a,1], Li Yang [a,1], Xia Mengyan [a], Cui Baoyu [a], Liu Chang [a], Du Xiuhong [c], Wang Zehua [a], Duan Xianying [d,e,*], Cui Jiehu [a,b,*]

[a] School of Materials science and Engineering, Zhengzhou University of Aeronautics, Zhengzhou, PR China
[b] Henan Engineering Research Center for Ceramic Materials Interface, Zhengzhou University of Aeronautics, Zhengzhou, PR China
[c] Clinical Laboratory Medicine, Henan Medical College, Zhengzhou, PR China
[d] School of Medicine, Huanghe Science and Technology University, Zhengzhou, PR China
[e] Institute of Chemistry, Henan Academy of Sciences, Zhengzhou, Henan 450002, PR China

ARTICLE INFO

Keywords:
ladyered double hydroxide (LDHs)
ZnCoCr-LDHs
Fluoride
Adsorption
TEA

ABSTRACT

Layered double hydroxides (LDHs) have attracted increasing attention as promising candidates by anion exchanges and selective adsorption in the fluoride treatment field. In this study, three new ternary Zn-Co-Cr-LDHs were synthesized by primarily a one-step TEA-assisted hydrothermal process at various times. They were characterized by X-ray powder diffraction, thermogravimetric analysis, scanning electron microscopy, X-ray photoelectron spectroscopy, N_2 gas adsorption and desorption curves and zeta potential. The effects of dosage amount, reaction duration, initial solution pH, temperature, and co-existing ions were evaluated systematically for the Zn-Co-Cr-LDHs in fluoride removal process. Compared to Zn-LDHs and Zn-Co-LDHs, three Zn-Co-Cr-LDHs showed excellent adsorption performance for F^- with maximum adsorption amounts of 108.87 mg/g, 97.27 mg/g, and 97.62 mg/g, respectively. The coexisting anions have less effect on the adsorption of F^-. The introduction Cr^{3+} ion modulation in the Zn-Co-LDHs greatly improved the adsorption of fluoride ions. The kinetic process of fluoride ion adsorption is in accordance with the quasi-secondary kinetic model and the Elovich model, and the adsorption isotherm is in accordance with the Langmuir model. The quasi-secondary kinetic and Elovich models suggest that the process is chemisorption-controlled ion exchange adsorption. Zn-Co-Cr-LDHs are expected to have potential applications in fluoride removal process.

1. Introduction

Fluoride is a vital component of natural water bodies and an essential trace element for the human body. Low concentrations of fluoride promote bone development and protect against dental caries in both children and adults (Ali et al., 2016). However, excessive intake of fluoride can lead to fluorosis (Zhang et al., 2022a,b). Fluorine pollution is also a global environmental problem, with at least 27 countries worldwide suffering from fluoride poisoning (Noor et al.,2022). Considering the intake of water and other sources, the World Health Organization recommends a daily guideline of 1.5 mg·L-1 (WHO 2017; Zhang et al., 2022a,b). Therefore, it is necessary to eliminate fluoride in high fluoride water through effective methods.

At present, the main fluoride removal technologies are precipitation (Mullen, 2005), electrochemical method (Singh et al.,2013), biological method (Hem, 1959), and membrane treatment (Xia et al.,2021). Due to high operating and maintenance costs, these methods remain a challenging task in removing F-applications (Ayoob and Gupta, 2006). However, adsorption method is widely used as a cheap and feasible technique (Susheela, 1999) . Among numerous natural and synthetic adsorbents, the formation of layered double hydroxides (LDHs) nanoparticles has attracted much attention due to their high specific surface area and high thermal stability (Fan et al., 2014) (Kang et al.,2017).

LDHs are composed of two layers of positively charged metal cations and an intermediate negatively charged anion, and widely used as environmentally friendly adsorbents (Wu et al.,2021). The wide choice of metal cations from one to four and interlayer anions has given rise to a series of layered functional materials. And monometallic hydroxides,

* Corresponding authors at: School of Materials science and Engineering, Zhengzhou University of Aeronautics, Zhengzhou, PR China.
E-mail addresses: dxynumber@163.com (D. Xianying), cuijiehu@163.com (C. Jiehu).
[1] These authors contributed equally to this work.

https://doi.org/10.1016/j.arabjc.2024.105645
Received 30 October 2023; Accepted 21 January 2024
Available online 23 January 2024

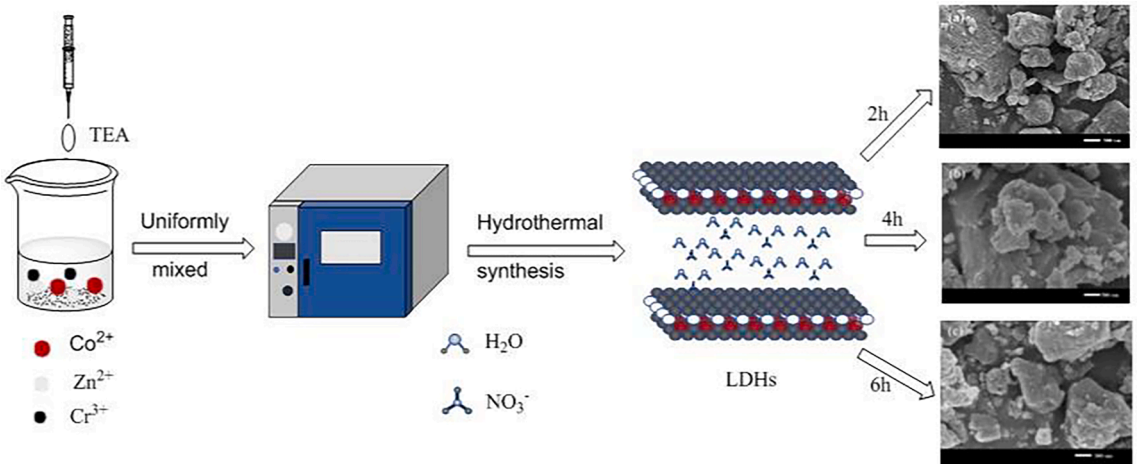

Scheme 1. The construction of ZCC-1, ZCC-2 and ZCC-3 by TEA-assisted hydrothermal method.

bimetallic LDHs and ternary LDHs have different adsorption effects (Liu et al.,2021). Moreover, when divalent ions are replaced by trivalent ions resulting in a net positive surface charge which is further counterbalanced by intercalated exchangeable anions. The net positive surface charge and availability of the exchangeable anions in the hydrated interlayer creates the high anion trapping capacity of LDHs (Zhang et al., 2022a,b). Our team first adopted triethanolamine (TEA) as a bifunctional alkali source and template to prepare some new LDHs as an efficient adsorbent by hydrothermal technology. However, so far, there are few studies on the modulation of adsorption performance by monometallic hydroxides, bimetallic LDHs and ternary LDHs for fluoride by TEA-assisted hydrothermal method. In addition, the enhanced adsorption mechanism also need to be further explored (Dang et al.,2023; He et al.,2012).

Based on the purpose of ensuring the safety of drinking water, in this paper, we prepared Zn-LDHs, Zn-Co-LDHs and three new ternary Zn-Co-Cr-LDHs for the removal of F^-. The experimental result shows that the introduction of Cr^{3+} into Zn-Co LDHs lead to greatly increasing F^- uptake. Therefore, the removal effect on F^- under different conditions, metal ion modulation effect were studied, and the adsorption mechanism was discussed in detail.

2. Experimental section

2.1. Materials

Zinc nitrate hexahydrate, cobalt nitrate hexahydrate, chromium nitrate nonahydrate, sodium chloride, triethanolamine (TEA), sodium citrate dihydrate, glacial acetic acid, sodium hydroxide, deionized water, anhydrous ethanol, sodium fluoride, (analytically pure).

2.2. Preparation of adsorbent

2.2.1. Preparation of Zn-LDHs

According to the subject literature (Li et al., 2022a; Zhu, 2022): The mixture of 0.01 mol zinc nitrate hexahydrate and 12 mL deionized water are stirred. 2 mL triethanolamine was added to the solution drop by drop and stirred for 10 mins. The mixture solution was placed it in the oven and kept 100 °C for 2 h. After cooling to room temperature, the mixture was solid–liquid separated by centrifuge, washed with deionized water and anhydrous ethanol for 3 times, then put into a drying, dried in oven and obtained Zn-LDHs.

2.2.2. Preparation of Zn-Co-LDHs

Zn-Co-LDHs were prepared using the same method as 2.2.1 by replacing 0.01 mol $Zn(NO_3)_2{\cdot}6H_2O$ using a total of 0.01 mol of zinc nitrate hexahydrate and cobalt nitrate hexahydrate in the ratio of 1:1 according to the subject literature (Li et al., 2022b; Zhu, 2022).

2.2.3. Preparation of three Zn-Co-Cr-LDHs

Three Zn-Co-Cr-LDHs were prepared using the same method as 2.2.1 by replacing 0.01 mol $Zn(NO_3)_2{\cdot}6H_2O$ using a total of 0.01 mol of Zn $(NO_3)_2{\cdot}6H_2O$, $Co(NO_3)_2{\cdot}6H_2O$ and $Cr(NO_3)_3{\cdot}9H_2O$ in the ratio of 1:1:2. The mixture was stirred well, then, 2 mL triethanolamine was added drop by drop under stirring, and next the mixture placed in a Teflon-lined stainless steel vessel in an oven at a reaction temperature of 100 °C from 2 h to 6 h. When the reaction was cooled to room temperature, three materials were separated, washed with deionized water and anhydrous ethanol and dried in a vacuum drying oven at 60 °C. Three nanomaterial were obtained after grinding, which are named as ZCC-1, ZCC-2 and ZCC-3, respectively.

In order to further verify the promoting effect of Cr^{3+}, Zn-Cr-LDHs and Co-Cr-LDHs were prepared using the above method for comparative experiments.

2.3. Characterization

ZCC-1, ZCC-2 and ZCC-3 were characterized using scanning electron microscopy (SEM, JSM-7001F), X-ray diffraction (XRD, BrukerD8-ANCE), Fourier infrared spectroscopy (FTIR, Thermo Fisher Nicolet IS5), X-ray photoelectron spectroscopy (XPS, Thermo ESCALAB 250Xi), N_2 adsorption–desorption isotherm testing (Micromeritics ASAP 2020), inductively coupled plasma emission spectroscopy (ICP, Agilent ICPOES 730), thermogravimetry (TG, Shimadzu DTG-60AH), zeta potential (Zetasizer Nano S) LDHs.

2.4. F^- adsorption experiments

Zn-LDHs, Zn-Co-LDHs, ZCC-1, ZCC-2 and ZCC-3 adsorbents were used to study the removal of F^- at low concentrations. The effects of different F^- concentrations, dosage, adsorption time, temperature, pH and coexisting anions on the removal of F^- were investigated.

20 mg adsorbent was added to 20 mL the F^- concentration of 500 mg/L, and the mixed solution pH were adjusted from 4 to 8 by adding 0.1 M HCl or NaOH solution. Then the mixed solution were placed on a stirrer at fixed temperature for constant time to reach adsorption equilibrium. Subsequently, ZCC was centrifuged and 10 mL of TISAB buffer was added to avoid the interference of cations such as aluminum, iron and silicon, and the volume was set to the mark. Finally, the concentration of F^- at equilibrium was measured by an ion selective electrode (Remag PF-2–01). The effect of co-existing anions such as $H_2PO_4^-$ (potassium salt), HCO_3^-, NO_3^-, SO_4^{2-} (sodium salt) on fluoride adsorption was also studied.

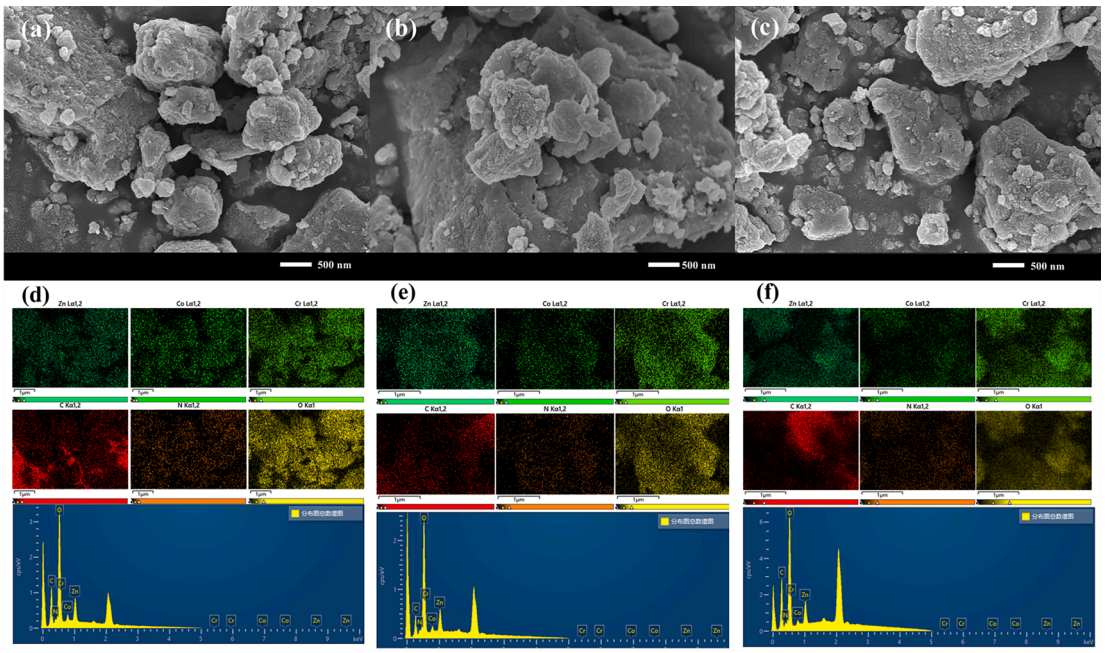

Fig. 1. SEM and EDS maps of ZCC-1, ZCC-2 and ZCC-3 (a-c) (d-f).

The adsorbent adsorption capacity (q_e) and removal rate (R%) for F^- were calculated using equations (1) and (2), respectively.

$$q_e = \frac{(C_0 - C_t) \times V}{m} \quad (1)$$

$$R\% = \frac{(C_0 - C_t)}{C_0}\% \quad (2)$$

Where: q_e: adsorption volume (mg/L); C_0: initial concentration (mg/L); C_t: equilibrium concentration (mg/L); m: the mass of adsorbent (mg); V: volume of solution (L).

3. Results and discussion

3.1. Characterization

Under hydrothermal conditions, three novel ternary Zn-Co-Cr-LDHs are schematically shown in Scheme 1 by the adjusting amount of TEA in the H_2O-TEA binary system at 120 °C from 2 to 6 h using $Zn(NO_3)_2$, $Cr(NO_3)_3$ and $Co(NO_3)_2$ as starting materials. ZCC-1, ZCC-2 and ZCC-3 were named based on the reactive time (2, 4, and 6 h, respectively). The morphology, microstructure and the component of ZCC-1, ZCC-2 and ZCC-3 were further investigated by SEM and EDS.

To investigate the changes in the surface morphology of the materials from Zn-LDHs, Zn-Co-LDHs to ZCC-3, three materials were analyzed by SEM and EDS in Fig. 1(a-f) and Fig.S1. Fig. 1 (a-c) shows that the three materials are consist of large irregular crystalline nanosheets which is difference from the quadrilateral structure of Zn-LDHs and the 3D flowerlike structure of Zn-Co-LDHs (Sahoo et al.,2019) which are stacked together by face-to-face contact, and the positive charges on the surface of the nanosheets and the negative charges on the edges of the nanosheets. They are in contact to form a sandwich structure by the stacking of ZCC irregular nanosheets (Lin et al.,2021). It can be seen that the layered structure and pores of the nanomaterials provide more space to keep more nitrate ions in order to make higher exchange capacity for the adsorption of F^- in the interlayer space, which is also shown ZCC may more anion exchange capacity than that of Zn-LDHs and Zn-Co-LDHs. The mapping plots of EDS detect the coexistence of O, Zn, Co, and Cr elements (Fig. 1d-f) in three materials as designed which further proves the successful synthesis of three ZCC nanomaterials.

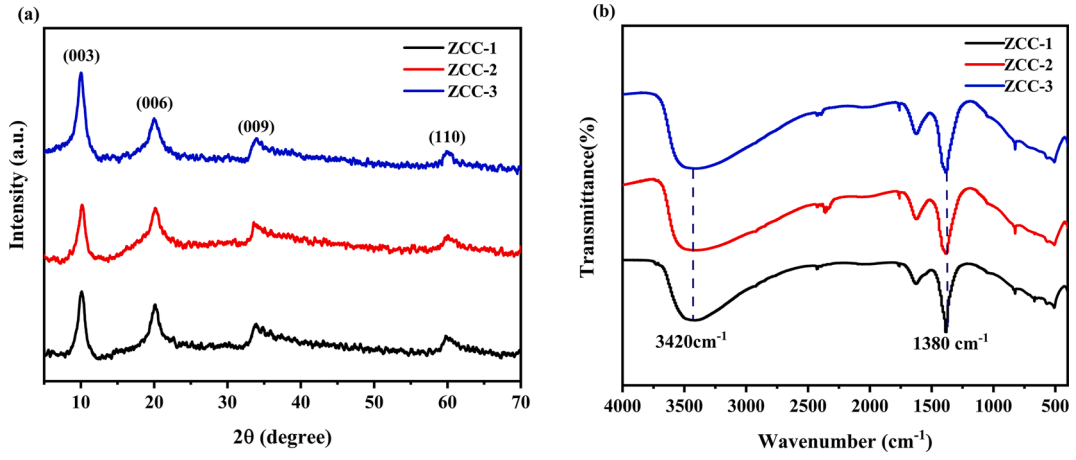

Fig. 2. XRD (a) and IR (b) plots of ZCC-1, ZCC-2 and ZCC-3.

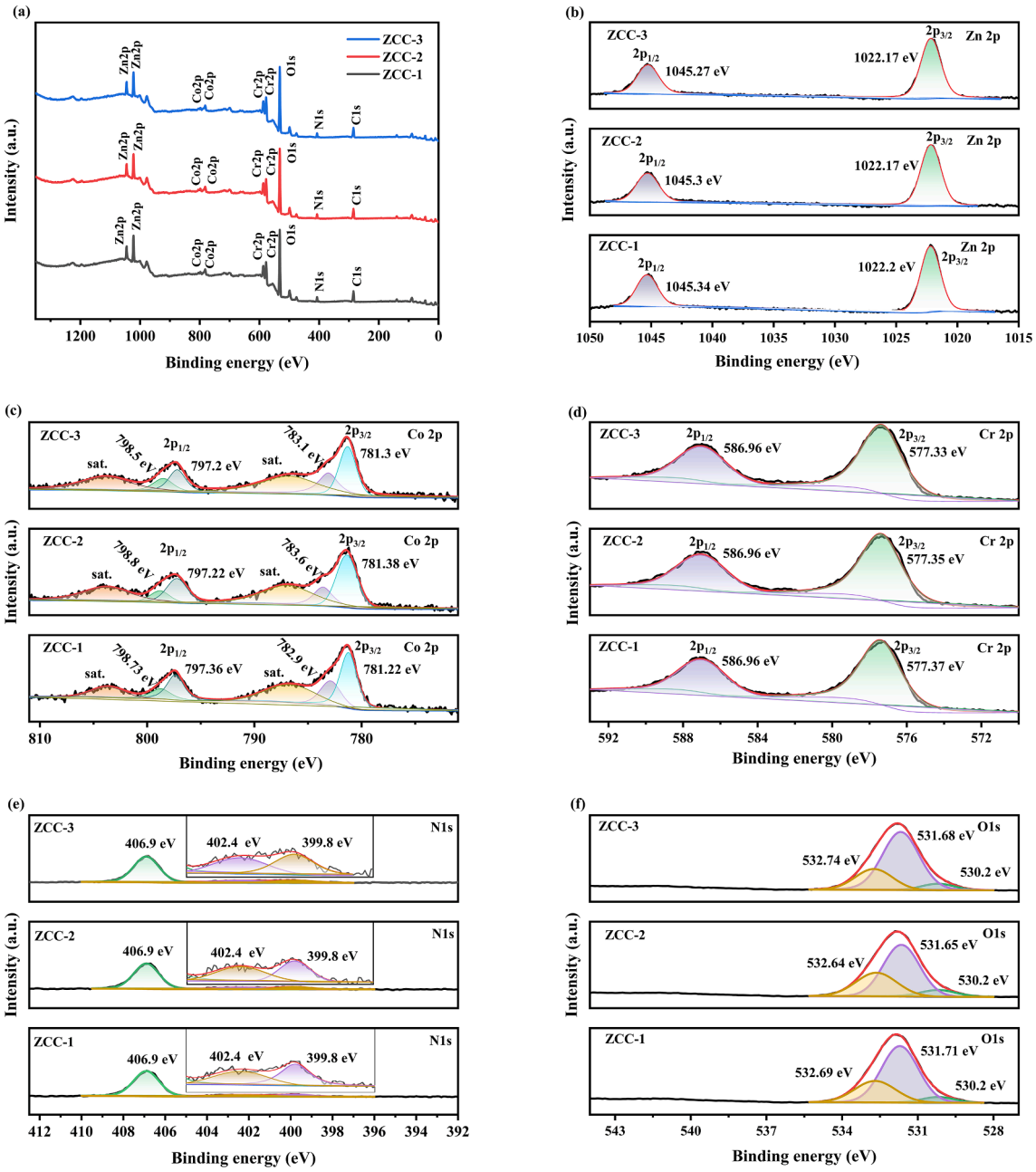

Fig. 3. Total spectrum of ZCC-1, ZCC-2 and ZCC-3 and XPS maps of (a) Zn, (b) Co, (c) Cr, (d) C, (e) N, (f) O elements.

The XRD patterns of the as-prepared three ZCC are represented in Fig. 2(a). As shown in Fig. 2(a), three materials all have indexed as (003), (006), (009) and (110) peaks located at 10.12, 20.11, 33.82 and 59.74° for ZCC-1, 10.16, 20.13, 33.58 and 60.01°for ZCC-2 and 10.04, 19.99, 33.93 and 59.91°for ZCC-3, respectively. Peaks at (003) for three ZCC which are typical characteristic peaks of LDHs are relatively sharp and demonstrated that three ZCC were successfully prepared (Kong et al.,2020). In addition, it can be also seen that no other peaks were detected which is proved the good crystallinity of three ZCC. Peaks at (003) as the base reflection of the interlayer anion is also indicated that the successful entry of NO_3^- ions into the interlayer in three ZCC LDHs (Mallakpour and Hatami, 2017). According to the Bragg equation ($n\lambda = 2d\bullet\sin(\theta)$), the d-values of c-axis for three ZCC at 10.12°, 10.16° and 10.04° are minor different (8.74, 8.70 and 8.80 Å, respectively).

For investigating the chemical structure, the functional groups of three ZCC were further analyzed by infrared spectroscopy (Fig. 2b). The broad peak at 3420 cm^{-1}, 1632 cm^{-1} and 1380 cm^{-1} is corresponds to the stretching vibration of the nitrate, the stretching vibration of the –OH group in the water molecules and the interlayer water molecule (Berner et al.,2018). The vibration absorbance peak at 1639 cm^{-1} is associated with the interlayer water molecules. Moreover, the higher intensity absorbance peak at 1380 cm^{-1} suggested the stretching vibration of NO_3^- in the ZCC interlayer which also confirms the presence of interlayer NO_3^- ions (Bekele et al.,2019) (Shinde et al.,2022), which also provides a side evidence of the higher stability of metal hydroxides than nitrates. The bands in the range 550–1200 cm^{-1} belong to the oxygen bonds of metal-LDHs lattices with M−O−M (Zn-O), (Co-O) and (Cr-O) groups such as Zn-O, Co-O-Co and Cr-O-Cr. The bands at 789 cm^{-1}, 571 cm^{-1} and 514 cm^{-1} belonging to the Cr-OH deformation mode. (Ma et al.,2021) (Mandal et al.,2013) The small peaks below 3000 cm^{-1} are stretching vibrations of $–CH_3$ and $–CH_2$ groups, confirming the existence of triethanolamine in the interlayer of LDHs(Liu et al.,2023).

XPS spectroscopy can be used to detect the surface elemental composition and bonding configuration of LDH. The element chemical

Table 1
Element mass percent of ZCC-1, ZCC-2 and ZCC-3 by ICP and elemental analyses.

material	Zn	Co	Cr	C	N	H
ZCC-1	13.0029 %	6.2258 %	23.3974 %	1.47 %	3.38 %	2.906 %
ZCC-2	11.6108 %	5.5547 %	23.6997 %	1.12 %	3.23 %	2.848 %
ZCC-3	11.9028 %	5.7191 %	25.1311 %	0.85 %	3.02 %	2.863 %

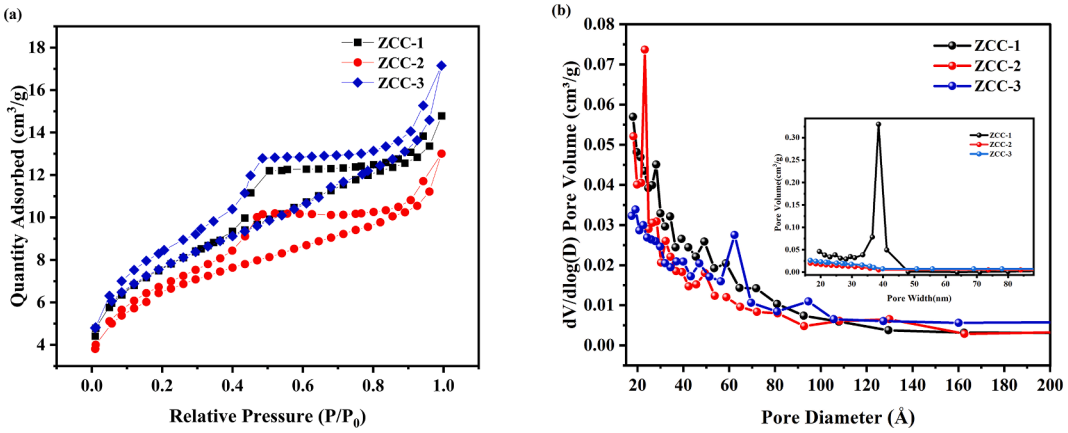

Fig. 4. N_2 adsorption and desorption curves (a) and pore size distribution (b) for ZCC-1, ZCC-2 and ZCC-3.

composition and chemical state of ZCC-1, ZCC-2 and ZCC-3 is further confirmed by XPS analysis in Fig. 3(a). From Fig. 3a, it can be seen that the full spectrum of three ZCC is further indicated the presence of Zn, Co, Cr, C, N and O elements based on C1s at 284.8 eV which is in agreement with the results of EDS elemental mapping. As shown in Fig. 3(b), the sharp peaks of element Zn 2p ($2p_{3/2}$ and $2p_{1/2}$) at binding energies 1022.2 eV and 1045.3 eV have a similar region and shape, demonstrating that Zn maintains the original Zn^{2+} electronic state for three ZCC. (Jie et al.,2022).

Four peaks can be observed for Co2p region of three ZCC by using a Gaussian fitting method in Fig. 3c. Two peaks at 782.9 eV and 798.73 eV are assigned to Co $2p_{1/2}$, two peaks at 797.36 eV and 781.22 eV are Co $2p_{3/2}$ orbits, and peaks at 803.7 eV, 786.7 eV. adjacent to the two main peaks are the corresponding satellite peaks; These data suggest that Co is present in ZCC-1 nanomaterials as Co^{2+} and Co^{3+}electronic state (Luo et al.,2019) (Li et al.,2021); As showed in Fig. 3d, the element Cr appears with peaks similar to those reported in the literature. Two peaks at 587.1 eV and 578.4 eV are Cr $2p_{1/2}$ and Cr $2p_{3/2}$ valence states, respectively. The additional peak detected at 577.1 is attributed to Cr^0 according to the binding energy handbook (Sahoo et al.,2018).

In Fig. 3e. The sharp N 1 s peaks at 399 eV in three ZCC is in the form of nitrate nitrogen and no graphitic nitrogen based on the N 1 s peaks of nitrate nitrogenat 399.6 eV and graphitic nitrogen at 406.4 eV. The O1s can be divided into three different peaks in Fig. 3f. The weak peak at 530.2 eV is caused by lattice oxygen in M−O−M, and other two peaks at 531.71 eV and 532.69 eV are attributed to the –OH group and O in NO_3^- as well as to chemisorbed water molecules (Bekele et al.,2019) (Dong et al.,2007) (An et al.,2012). The peaks of C1S at 284.80 eV in all ZCC are consistent with the standard binding energy.

For determining the molecular formula of three ZCC, the ratios of Zn, Co and Cr were analyzed using ICP, and C, N and O elements were determined by elemental analysis. As shown in Table 1, The results accurately show the Zn/Co/Cr and C/ N/ O ratio of three ZCC which was also consistent with the EDS results.

Table 2
Specific surface area, pore size and pore volume of ZCC-1, ZCC-2 and ZCC-3.

material	BET surface area (m^2 /g)	Pore volume (cm^3 /g)	Pore size (nm)
ZCC-1	27.3144	0.022867	36.403
ZCC-2	23.4057	0.020119	34.659
ZCC-3	27.3413	0.026532	36.757

Based on the ICP measurements, the molar ratio of M^{2+} /M^{3+} is close to the initial ratio, which further proves the effective synthesis by hydrothermal method; Combined with the results of ICP, elemental analysis, TG analysis and the chemical general formula, the chemical formulae of three ZCC were calculated as $[Zn_{0.354}Co_{0.173}Cr_{0.473}(OH)_2]\cdot_{0.473}[NO_3^-]_{0.473}\cdot 0.411H_2O$, $[Zn_{0.333}Co_{0.162}Cr_{0.505}(OH)_2]_{0.505}[NO_3^-]_{0.505}\cdot 0.396H_2O$ and $[Zn_{0.327}Co_{0.160}Cr_{0.513}(OH)_2]_{0.513}[NO_3^-]_{0.513}\cdot 0.371H_2O$.

According to the IUPAC classification, three ZCC can be classified as type IV with H_4 hysteresis rings (Fig. 4a), indicating that all three ZCC are mesoporous and aggregated crystals formed by layer-by-layer lamellar contacts of LDHs (El Hassani et al.,2017). Such results are correspond to the SEM analysis. The parameters of surface area and pore structure are shown in Table 2. As seen in Table 2, the reaction time does not have much effect on the specific surface area, pore volume and pore diameter of ZCC-1, ZCC-2 and ZCC-3. The BET surface area of ZCC-1 and ZCC-3 are 27.3144 and 27.3413 $m^2\cdot g^{-1}$. The pore volume of ZCC-1 and ZCC-3 is 0.022867 and 0.026532 $cm^3\cdot g^{-1}$, and the pore diameter are 36.403 and 36.75 nm, respectively. The pore sizes are concentrated between 0 and 50 nm, indicating that three ZCC are all mesoporous materials (Tan et al.,2019). Compared with ZCC-1 and ZCC-3, ZCC-2 possessed the smallest specific surface area, pore volume and pore diameter which were 23.41 m^2 /g, 0.02 cm^3 /g and 34.66 nm, respectively. According to Fig. 4b and Table 2, ZCC-1 had a partially larger pore width with the mesoporous pores of 0–50 nm, which was the reason that the specific surface area and pore volume of ZCC-1 were slightly lower than those of ZCC-3, but the adsorption amount was larger than that of ZCC −3 which is due to the larger adsorption capacity.

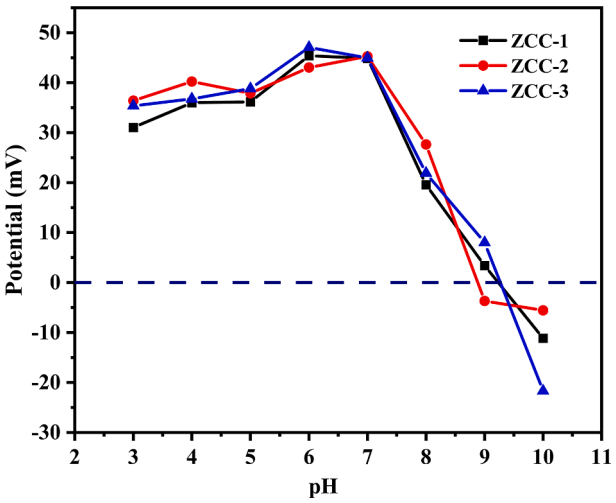

Fig. 5. Zeta potential analysis of ZCC-1, ZCC-2 and ZCC-3.

Thermogravimetric analyses show (Fig. S2) that all three ZCC have all three heat-absorbing and one exothermic peak with the same thermal decomposition process, differing slightly in temperature. For the ZCC-1 (Fig. S2a), the weight loss at 80–130 °C is due to the loss of interlayer water molecules of the material and the structure of the material is not destroyed; the two heat absorption peaks at 200–350 °C are attributed to the dehydroxylation of LDHs and the decomposition of interlayer NO_3^-; the exothermic peak at 390–410 °C is attributed to the decomposition of the ZCC-1 and the transformation of LDHs to LDOs(Xu et al.,2022; Zeng et al.,2022; Yang et al.,2023).

The zero potential was determined using a zeta potential meter in order to understand the surface charge of three ZCC, and the results are shown in Fig. 5. The zero potential values of three ZCC were positively charged over a wide pH range from 3 to 10, offering the more adsorption capacity between anionic contaminants and ZCC by electrostatic interaction. The zero-point potentials of ZCC-1, ZCC-2 and ZCC-3 when pH values > 9.28, 8.88 and 9.27 were negatively charged , which will hinder surface adsorption through electrostatic attraction.

3.2. Adsorption performance of Zn-Co-Cr-LDHs on F

3.2.1. The adsorption performance of Zn-LDHs, Zn-Co-LDHs and Zn-Co-Cr-LDHs on F

In order to design and prepare new LDHs with higher adsorption performance by the expansion of single metal, binary metal to ternary metal LDHs, and the adsorption performance of Zn-LDHs, Zn-Co-LDHs, Co-Cr-LDHs, Zn-Cr-LDHs, ZCC-1, ZCC-2 and ZCC-3 on F^- were executed. 15 mg adsorbent were dispersed in 20 mL of NaF solution with a concentration of 20 mg/L at pH = 5 in a test tube at room temperature for 1 h. The removal rate of Zn-LDHs, Zn-Co-LDHs, Co-Cr-LDHs, Zn-Cr-LDHs, ZCC-1, ZCC-2 and ZCC-3 for F^- are shown in Fig. 6. The results showed that the adsorption rates of Zn LDHs and Zn-Co-LDHs for F^- were 27.51 % and 30.44 %, respectively. The addition of Cr^{3+} greatly improved the defluorination rate, while the defluorination rates of CoCr LDHs and ZnCr LDHs increased to 90.09 % and 94.17 %, respectively. The ternary ZCC adsorbent had the best effect, with 97.26 %, 97.25 %, and 97.70 %, respectively. It can be seen that the removal rate is an obvious enhancement after the introduce of Cr cation which is due to morphology and pore diameter changes for ZCC-1, ZCC-2 and ZCC-3, so

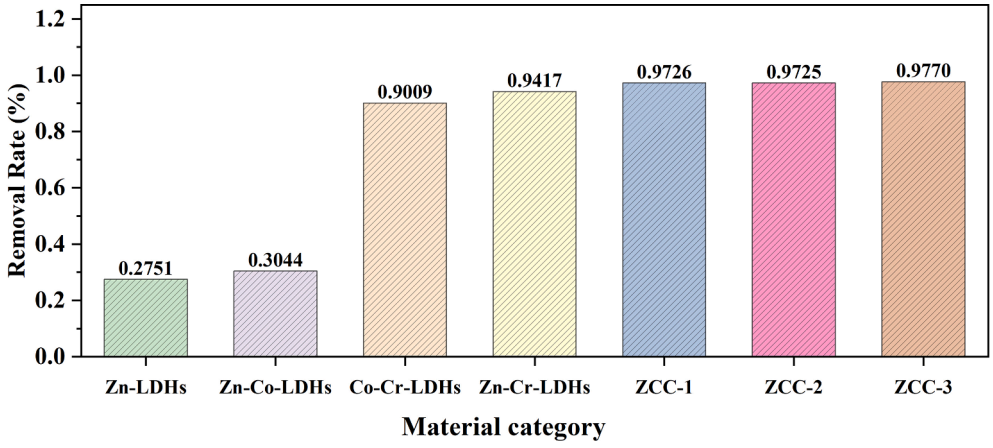

Fig. 6. Removal rates of Zn-LDHs, Zn-Co-LDHs, ZCC-1, ZCC-2 and ZCC-3 on F^-.

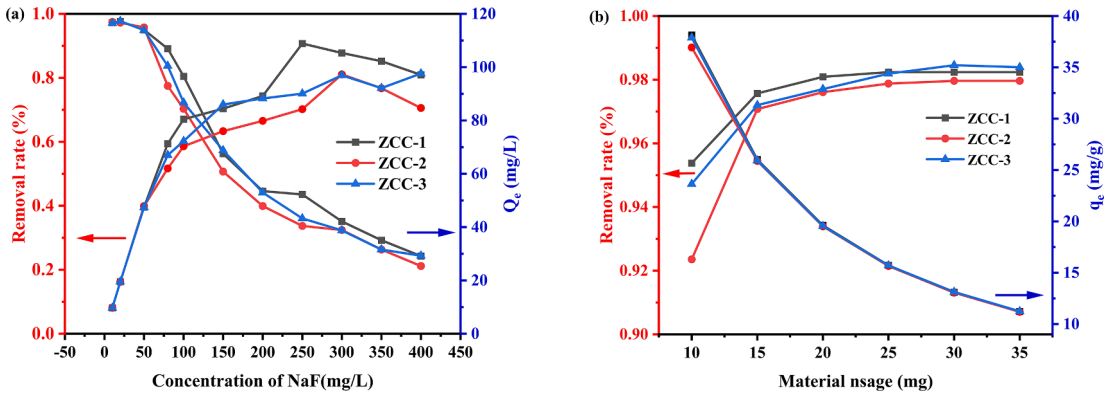

Fig. 7. Variation of removal and adsorption of F^- by ZCC adsorbent at different concentrations (a) and dosing levels (b).

Table 3
Maximum adsorption capacity of three ZCC adsorption F^- compared with other adsorbents.

Adsorbent	Q_m (mg/g)	References
EG/LDHs expanded graphite/laminated double hydroxide	63.21	Zheng et al., 2023
LALDH-201	62.5	(Cai et al.,2016)
$ZnCr_3$ –NO_3 -LDH	31	(Koilraj and Kannan, 2013)
Mg/Fe-CLDH	50.91	(Kang et al.,2013)
HTlcMA-EDA	22.47	(Coyote-Jiménez et al.,2021)
ZCC-1	108.87	this work
ZCC-2	97.27	this work
ZCC-3	97.62	this work

the exploration of the optimal conditions of adsorbent on the removal of F^- was next adopted using ZCC-1, ZCC-2 and ZCC-3 as the center.

3.2.2. *Initial concentration and adsorbent dosage*

The effect of initial F^- concentration is a significant effect factor in the adsorption process by three ZCC. Other conditions such as pH, adsorbent dosage, volume and stirring rate were fixed. The adsorbent dosage was controlled at 20 mg, and the initial concentration of the solution was varied from 10 mg/L to 400 mg/L. All tests were performed at room temperature (298 ± 1 K), and the experimental results are shown in Fig. 7a.

As the initial solution concentration of F^- increased from 10 mg/L to 400 mg/L, the removal of F^- by ZCC-1, ZCC-2, and ZCC-3 decreased from the initial 97.26 %, 97.46 %, and 97.14 % to 24.28 %, 21.17 %, and 24.41 %, respectively, and the adsorption amounts of the materials were saturated with a maximum of 108.87 mg/g, 97.27 mg/g, 97.62 mg/g. It can be seen from the data that the removal rate is high at low fluorine concentration from 10 to 300 mg/L. While, the removal rate decreases when the initial concentration increased from 300 to 400 mg/L. The reason may be that the amount and adsorption sites of ZCC-1, ZCC-2, and ZCC-3 are certain, and the adsorbed amount increases with the increase of the solution concentration which leads to more and more reactive adsorption site were occupied in ZCC. Therefore, with the increasing remaining F^- concentration, the removal rate decreases and the maximum adsorption capacities are reached.

Comparing to the maximum adsorption capacities of other adsorbents reported toward F^-, in this paper, the adsorption capacity of ZCC on F^- is superior to that of some adsorbents such as $ZnCr_3$-NO_3-LDH, Mg/Fe-CLDH. ect (Table 3), so ZCC-1 can be considered to be excellent candidate for the remove of F^-.

Fig. 7 (b) presents the effect of ZCC dosage from 10 to 35 mg on the adsorption performance on F^-. As seen in Fig. 7b, the removal rate increases and reach equilibrium as the amount of adsorbent used increases which may be due to the increase in active sites in adsorption process with increasing amount of adsorbent (Jie et al.,2022). While, the adsorption amounts gradually decreased from to 26.02 mg/g, 25.89 mg/g and 25.92 mg/g because of the increase of ZCC dosage, This indicates that ZCC showed excellent adsorption performance on F^-. The removal rate was higher than 97 % at 15 mg, and so the fixed adsorbent dosage was 15 mg for further study.

3.2.3. *Effect of reaction time, pH and temperature*

The adsorbent dosage was controlled at 15 mg and the initial concentration was fixed at 20 mg/L, the reaction time was varied from 0 to 120 min, and the experimental results were shown in Fig. 8a.

As shown in Fig. 8a, the adsorption of F^- by ZCC-1, ZCC-2 and ZCC-3 is a fast adsorption process and the removal rates of ZCC-1 and ZCC-2 reached 93.64 % and 95.13 % at 1 min, and the adsorption amounts reached 24.97 mg/g and 25.37 mg/g, respectively. Compared with ZCC-1 and ZCC-2, the removal rate of ZCC-3 at 1 min was only 91.2 % and the adsorption amount was 24.32 mg/g. With the increase of adsorption time, the adsorption effect of ZCC-1, ZCC-2 and ZCC-3 gradually smoothed out and attained a dynamic equilibrium which was due to there are no more active sites of the adsorbent under the premise with the increased of the reaction time when the adsorbent were certain. This result was also consistent with that of Langmuir model. In order to ensure sufficient contact between the adsorbent and the solvent, the adsorption time was fixed at 1 h for further study.

The pH of 20 mg/L NaF solution was adjusted to 4, 5, 7 and 8 (±0.02)

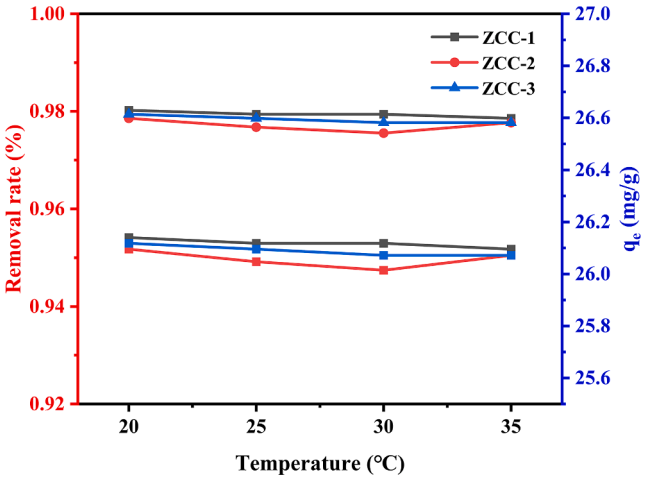

Fig. 9. The removal variation of f^- and adsorption capacity of ZCC adsorbent at different temperatures.

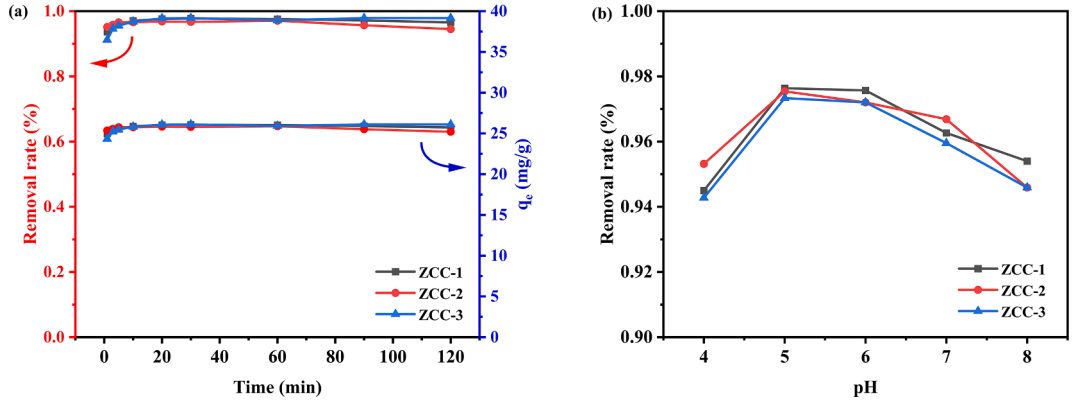

Fig. 8. Variation of removal and adsorption of F^- by ZCC adsorbent at different reaction times (a) and pH (b).

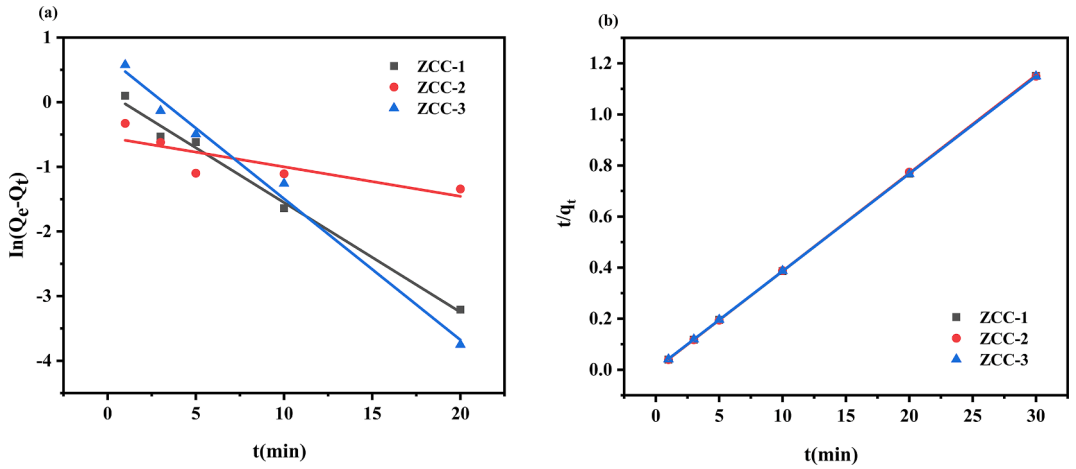

Fig. 10. Quasi-primary kinetic (a) and quasi-secondary kinetic (b) evaluation of the removal of f⁻ by ZCC sorbents.

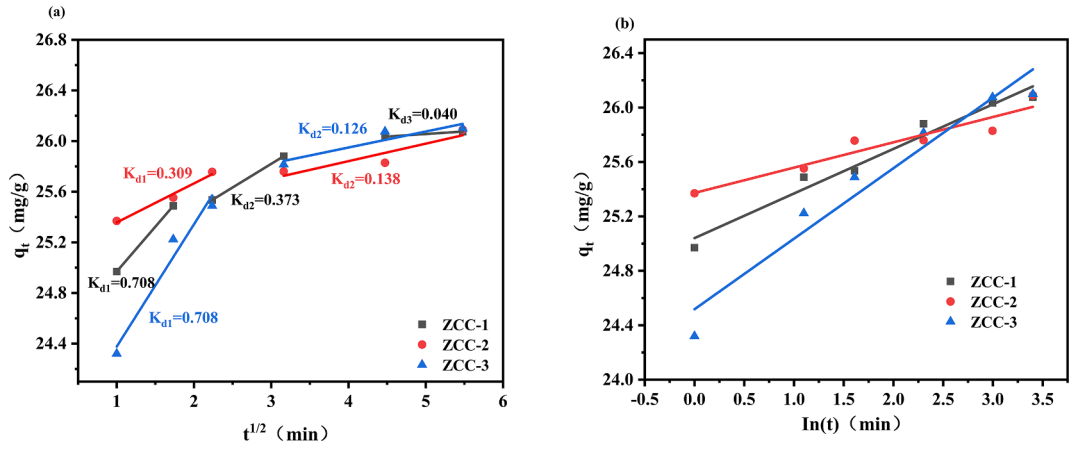

Fig. 11. Evaluation of intraparticle diffusion (a) and elovich model (b) for the removal of f- by zcc adsorbents.

with low concentrations of HCl and NaOH. Then 15 mg of adsorbent was added and the reaction was carried out on a magnetic stirrer for 1 h. The results of the removal rate are shown in Fig. 8 b.

With the increase of pH from 4 to 8, the removal rate of F^- showed a trend of increasing and then decreasing. there are the highest removal rates of F^- with 97.638 %, 97.541 % and 97.335 % for ZCC-1, ZCC-2 and ZCC-3, respectively; ZCC-1, ZCC-2 and ZCC-3 all maintained an overall removal rate of more than 94 % at different pH values, indicating that three ZCC is applicable to a wide range for the adsorption of F^-. In addition, the high removal rate of F^- may be related to the positive charge of the adsorbent in the pH = 4 to 8 medium which is in agreement with the zeta potential measurements. The fixed solution pH = 6 (i.e., using the configured 20 mg/L NaF solution) was further explored.

Other conditions such as pH, adsorbent dosage, the initial concentration, volume and stirring rate were fixed, and the reaction temperatures were varied from 20 °C, 25 °C, 30 °C to 35 °C. The experimental results are shown in Fig. 9.

From the experimental results, the change of temperature had a small effect on the adsorption of F^- by the materials, and all three materials maintained a fluoride removal rate above 96 %; with the increase of temperature, the three adsorbents maintained an overall decreasing trend for fluorine adsorption, and the maximum removal rates were 98.03 %, 97.86 %, and 97.94 %, respectively, and the adsorption amounts floated within 26 ± 1 mg/g without significant changes.

3.2.4. Adsorption kinetics

The adsorption kinetics were used to investigate the adsorption rates and adsorption mechanisms of ZCC-1, ZCC-2 and ZCC-3 on F^-. using different kinetic models such as: linear regression using quasi primary kinetic model, quasi secondary kinetic model, intraparticle diffusion model and Elovich model.

Table 4
Adsorption kinetic analysis of ZCC adsorbents for the removal of F^-.

material	quasi-level dynamics (physics)			quasi-secondary dynamics (physics)		
	Q_e	K_1	R^2	Q_e	K_2	R^2
ZCC-1	1.1539	0.16954	0.99086	26.1370	0.46178	1
ZCC-2	0.5805	0.0456	0.70241	26.0900	0.50312	0.99996
ZCC-3	1.9970	0.21847	0.99027	26.1986	0.33188	0.99999

Quadratic kinetic equation.

$$In(q_e - q_t) = Inq_e - k_1 t \tag{3}$$

Quasi-secondary kinetic equation.

$$\frac{t}{q_t} = \frac{1}{k_2 q_e^2} + \frac{t}{q_e} \tag{4}$$

Intraparticle diffusion model.

$$q_t = k_i t^{1/2} + C_i \tag{5}$$

Elovich model.

Table 5
Adsorption kinetic analysis of ZCC adsorbents for the removal of F^- (2).

material	Intraparticle diffusion			Elovich model		
	K_1	K_2	K_3	α_E	β_E	R^2
ZCC-1	0.708	0.373	0.040	4.80135E + 32	3.0497	0.96858
ZCC-2	0.309	0.138	–	3.18371E + 58	5.3755	0.91099
ZCC-3	0.708	0.126	–	1.80599E + 20	1.9292	0.9467

$$q_t = \frac{1}{\beta_E} In(\alpha_E \beta_E) + \frac{1}{\beta_E} Int \quad (6)$$

where: q_t, q_e: adsorption capacity at moment t and at equilibrium, mg/g. t: adsorption time, min. k_1, k_2, k_i: the rate constants of the model. C_i: the coordinate intercept of the linear fit. α_E, β_E: indicate the rate constants for suction/desorption.

The adsorption experimental data for ZCC-1, ZCC-2 and ZCC-3 were fitted using four kinetic models. The linear regressions and fitting parameters are shown in Figs. 10-11 and tables 4-5.

From the adsorption kinetic fit data (Figs. 10-11), it can be seen that the ZCC-1, ZCC-2 and ZCC-3 adsorbent materials more fit well with the quasi-secondary kinetic model with correlation coefficient $R^2 > 0.99$ which shown the adsorption reaction kinetics may be controlled by chemisorbed and ion exchange.

The adsorption kinetic fit data by Elovich model indicates that the adsorbent solid surface is inhomogeneous which is also consistent with the SEM observation that the interaction between the adsorption and desorption processes does not fundamentally affect this adsorption kinetic process when the adsorbent molecules are covered on its surface (Gupta and Bhattacharyya, 2011).

Furthermore, the two-stage diffusion of ZCC-2 and ZCC-3 are surface diffusion and internal diffusion, respectively. In addition to surface diffusion, ZCC-1 also clearly exhibits mesoporous and microporous diffusion. The kinetic data by intraparticle diffusion cannot be satisfactorily fitted which indicates that intraparticle diffusion is not key contribution in the adsorption process of fluoride onto synthetic LDHs (Mandal et al.,2013).

3.2.5. Adsorption isotherm

Adsorption isotherms provide qualitative information about the capacity of the adsorbent and the nature of solute-surface interactions (Jie et al.,2022), the Langmuir adsorption isotherm model (7) and the Freundlich adsorption isotherm model (8) were used to fit the adsorption isotherm data by the linear regression. The fitting kinetic parameters for F^- adsorbed by three ZCC are shown in Fig. 12 and Table 6, respectively.

Langmuir adsorption isotherm model.

$$\frac{C_e}{Q_e} = \frac{1}{Q_m K_L} + \frac{C_e}{Q_m} \quad (7)$$

Freundlich adsorption isotherm model.

$$InQ_e = InK_F + \frac{1}{n} InC_e \quad (8)$$

Where: Q_e, Q_m - fluorine adsorption/maximum adsorption capacity of the adsorbent, mg/g; C_e - concentration of fluoride ions remaining in solution at reaction equilibrium, mg/L; K_L - Langmuir's adsorption constant. K_m, n- Freundlich's adsorption constants.

As can be seen from the fitted data (Fig. 12), the R^2 values fitted by the Langmuir adsorption isotherm model for ZCC-1, ZCC-2 and ZCC-3 (0.99451, 0.9922, 0.99777) are larger than the R^2 values fitted by the Freundlich adsorption isotherm model (0.85801, 0.87158, 0.87499), indicating that the adsorption isotherms for F^- are more consistent with the Langmuir equation. The maximal adsorption capacities for F^- by ZCC-1, ZCC-2 and ZCC-3 are calculated to be 101.7294, 89.9281, 96.8054 $mg \cdot g^{-1}$ which is nearly consistent with that obtained by experiments.

The Langmuir model is based on the following assumptions(özcan et al.2009) (1) the adsorbent molecules are adsorbed as a monolayer on the adsorbent surface; (2) there is no force between the adsorbent and adsorbed molecules (3) the final equilibrium reached by the adsorption reaction is a dynamic equilibrium; the theoretical maximum adsorption amount calculated from the equation is closer to the actual theoretical adsorption amount; the obtained K_L values are all between 0 and 1, indicating that the adsorption of F^- is good and consists mainly of uniform adsorption patches(Jie et al.,2022); and the experimental results of reaction time also corroborate that the adsorption of ZCC-1, ZCC-2 and ZCC-3 on F^- is a dynamic equilibrium process.

3.2.6. Adsorption thermodynamics

The temperature is important effect on the adsorption of F^- and its effect were evaluated at 293, 298, 303 and 308 K. Adsorption thermodynamic parameters such as the enthalpy change (ΔH), entropy change

Table 6
Adsorption isotherm analysis of ZCC adsorbents for the removal of F^-.

material	Langmuir adsorption isotherm model			Freundlich adsorption isotherm model		
	Q_m	K_L	R^2	n	K_F	R^2
ZCC-1	101.7294	0.2564	0.99451	3.4764	24.8903	0.85801
ZCC-2	89.9281	0.1836	0.9922	3.7352	23.1689	0.87158
ZCC-3	96.8054	0.1726	0.99777	3.5696	23.6793	0.87499

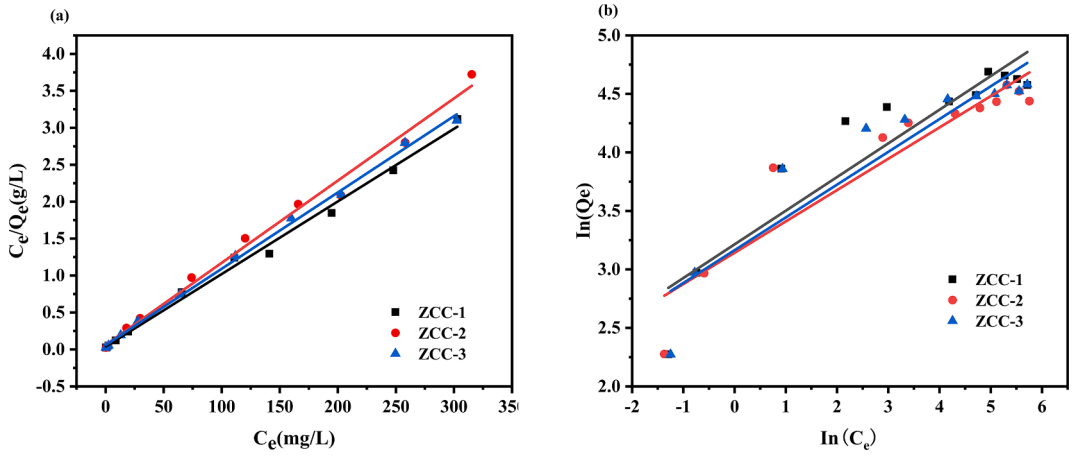

Fig. 12. Adsorption isotherm model for removal of F^- by ZCC adsorbents (a) Langmuir adsorption isotherm model (b) Freundlich adsorption isotherm model.

Table 7
Thermodynamic analysis of the adsorption of ZCC adsorbents for the removal of F^-.

Material	Reaction temperature	Initial concentration /(mg/L)	Equilibrium concentration /(mg/L)	Sorption potential (KJ/mol)	ΔG	ΔH	ΔS
ZCC-1	293	20	0.3951	9.5599	−8.4686	−3.6443	25.7937
	298	20	0.4114	9.6228	−8.6132		
	303	20	0.4114	9.7842	−8.7577		
	308	20	0.4284	9.8420	−8.9022		
ZCC-2	293	20	0.4284	9.3627	−9.0991	−2.6816	28.7668
	298	20	0.4645	9.3219	−9.2543		
	303	20	0.4891	9.3484	−9.4096		
	308	20	0.4461	9.7384	−9.5649		
ZCC-3	293	20	0.4114	9.4613	−8.6957	−4.2715	26.0334
	298	20	0.4284	9.5225	−8.8440		
	303	20	0.4461	9.5803	−8.9924		
	308	20	0.4461	9.7384	−9.1408		

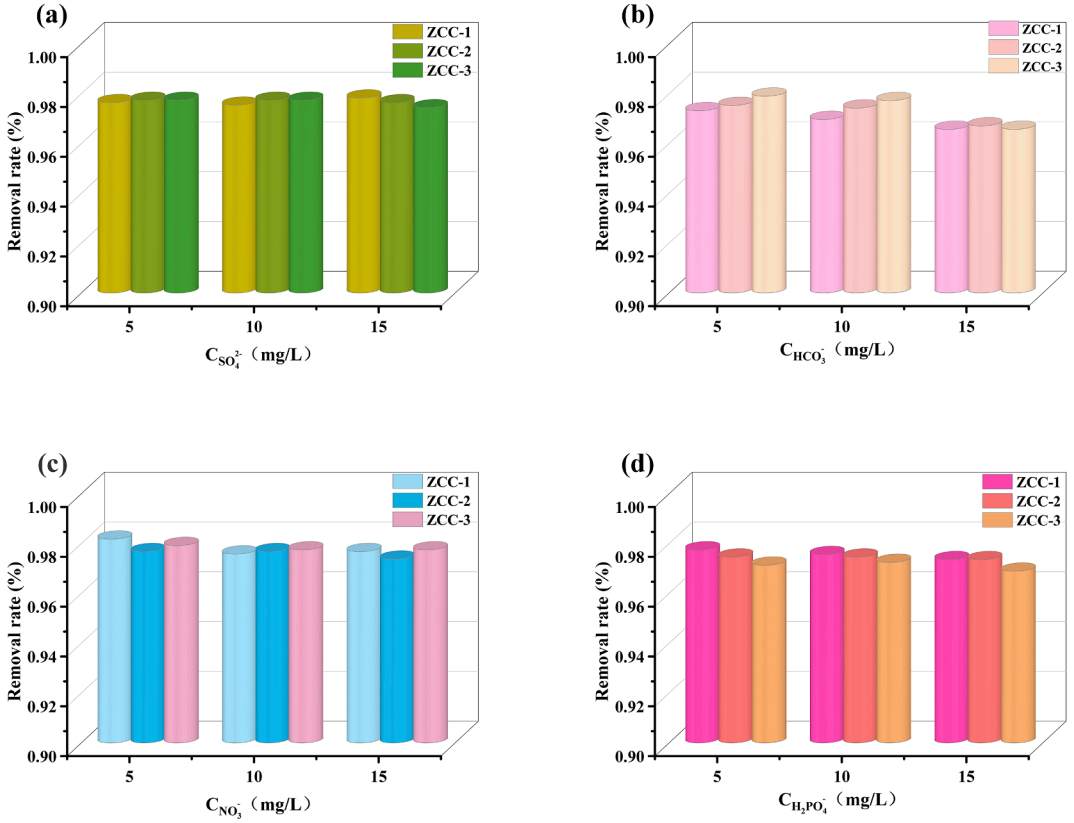

Fig. 13. Effect of other interfering ions (a) SO_4^{2-} (b) NO_3^- (c) HCO_3^- (d) $H_2PO_4^-$ on the adsorption of fluoride ions by three ZCC.

(ΔS) and Gibbs free energy (ΔG) by ZCC-1, ZCC-2 and ZCC-3 at 293, 298, 303 and 308 K were calculated by the following equations (9–11).

The enthalpy change (ΔH) is calculated from the Clausius-Clapeyron equation.

$$lnC_e = \Delta H/RT + lnK_0 \quad (9)$$

The entropy change (ΔS) can be calculated from the Gibbs-Helmholtz equation as

$$\Delta S = (\Delta H - \Delta G)/T \quad (10)$$

The Gibbs free energy (ΔG) is calculated by substituting the Gibbs equation into the Freundlich equation as follows.

$$\Delta G = -nRT \quad (11)$$

The adsorption potential (E) is calculated using the Polanyi adsorption theory equation.

$$E = -RTln(C_e/C_0) \quad (12)$$

where: R - ideal gas state constant. T - reaction temperature, K. C_0 - the initial concentration of the solution. K_0 - a constant.

The calculated ΔH by plotting and fitting lnC_e against 1/T is negative, indicating that the adsorption reactions of ZCC-1, ZCC-2 and ZCC-3 on F^- are exothermic processes and the adsorption amount varies negatively with the ambient temperature. $\Delta H < 0$ and $\Delta S > 0$ indicated that the reaction was an exothermic reaction with an increase in entropy. $\Delta G < 0$ indicated that the reaction was spontaneous (Table 7).

The adsorption potential (E) is an important parameter to distinguish between physical and chemical adsorption. When $E < 8$ kJ/mol, the adsorption process is physical adsorption; when E is between 8 and 16 kJ/mol, the adsorption process is ion exchange adsorption; when $E > 20$ kJ/mol, the adsorption process is chemical adsorption. The adsorption potentials of ZCC-1, ZCC-2 and ZCC-3 on F^- are greater than 8 kJ/mol and less than 16 kJ/mol, which are ion exchange adsorption (Li

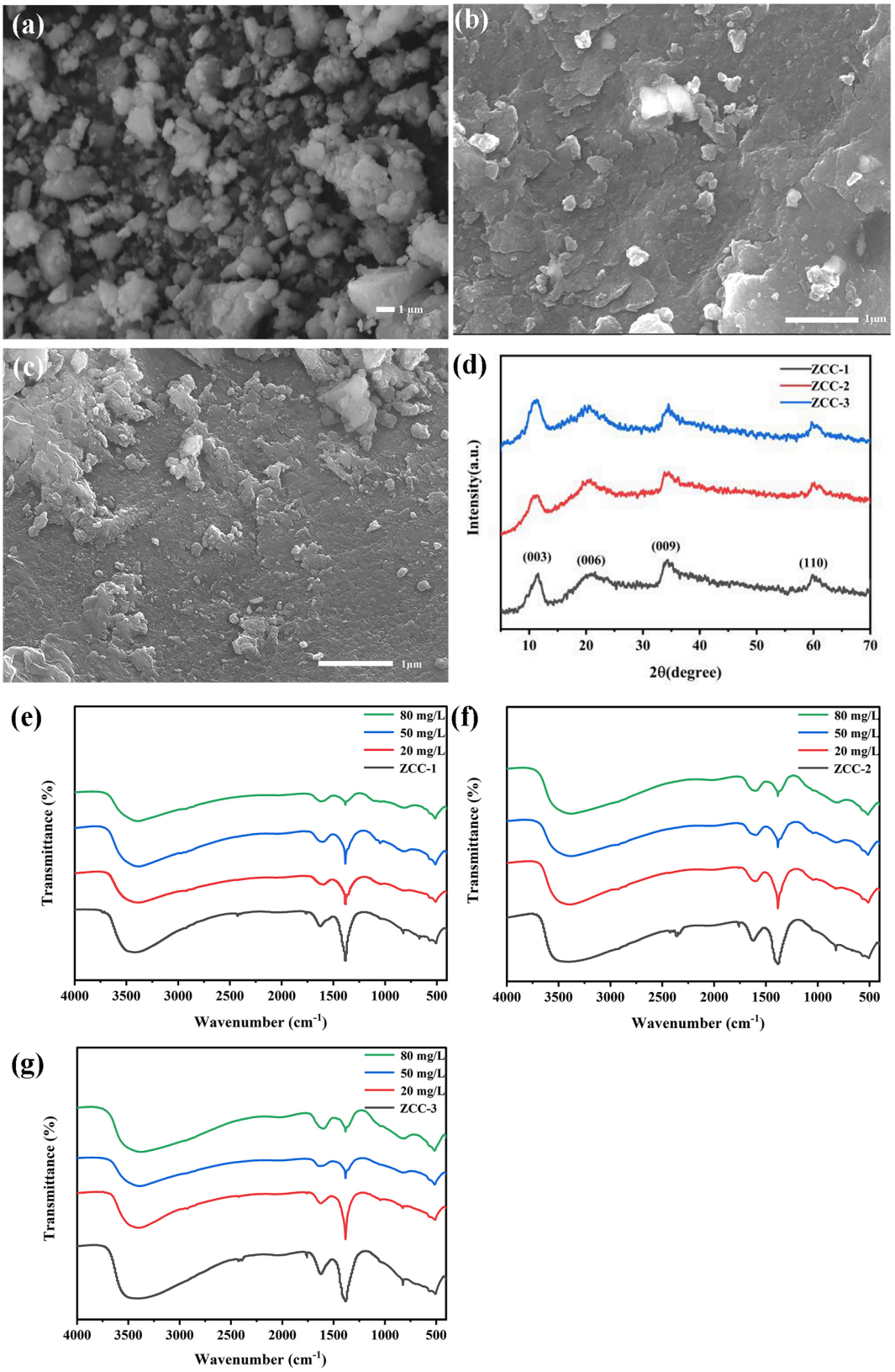

Fig. 14. SEM (a-c), XRD (d) and IR(e-f) plots of ZCC-1, ZCC-2 and ZCC-3 after adsorption.

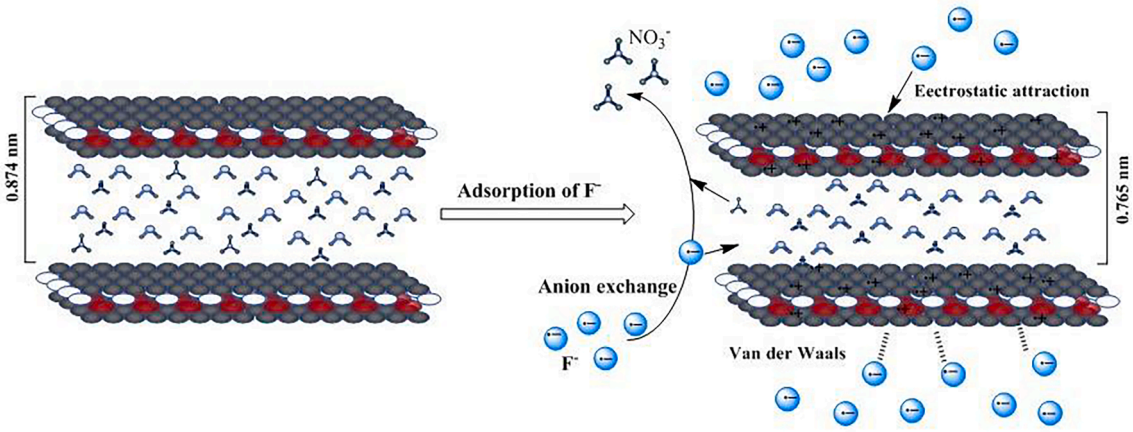

Scheme 2. Schematic analysis of the adsorption mechanism.

et al.,2019). The adsorption potentials of all three materials for F^- were in the range of 8 to 16 kJ/mol, and the main type of reaction was interlayer anion exchange.

3.2.7. *Effect of coexisting anions*

The effect of other coexisting anions such as $H_2PO_4^-$ (potassium salt), HCO_3^-, NO_3^-, SO_4^{2-} (sodium salt) on the adsorption of fluoride ions by ZCC-1, ZCC-2 and ZCC-3 was studied. The concentration of coexisting anions varies from 5 to 15 mg/L for 15 mg of ZCC-1, ZCC-2 and ZCC-3. The results of the experiment are shown in Fig. 13.

The experimental results showed that the adsorption rate of F^- did not change significantly in coexistence with other solutions of different concentrations of anions around 97 %, indicating that low concentrations of interfering anions have less effect on the adsorption of F^- by ZCC-1, ZCC-2 and ZCC-3. Compared to other coexisting ions, the adsorption of fluoride ions is also a selective adsorption by ZCC-1, ZCC-2 and ZCC-3.

3.3. *Analysis of adsorption mechanism*

The adsorption mechanism of F- by ZCC-1, ZCC-2 and ZCC-3 was further investigated by SEM, XRD and FTIR. As illustrated in Fig. 14a-c, after the adsorption process, the surface morphology of ZCC-1, ZCC-2, and ZCC-3 underwent a transformation from uneven and irregular crystal nanosheets to a smoother appearance. This change could be attributed to the occupation of the surface pores by F^-. Following the adsorption process (see Fig. 14d), the three ZCC nanomaterials still exhibited the characteristic peaks of LDHs, although the intensity of the peaks decreased significantly. The peak at (003) shifted from left to right, and the peak shape at (006) widened significantly. This is due to the replacement of the smaller radius NO_3^- by F^- through interlayer ion exchange, causing lattice distortion of LDHs (Berner et al., 2018). As a result, the interlayer spacing decreased from 0.874, 0.870, and 0.880 nm to 0.765, 0.785, and 0.777 nm, which aligns with the structural analysis of SEM.

Fig. 14e-g shows that the NO_3^- peak value at 1380 cm-1 did not change after adsorption, but its intensity decreased with increasing F-concentration. This is due to the exchange between F^- and NO_3^-. The NO_3^- content decreased gradually, which is an indication that the F^- adsorption process is mainly ion exchange.

Three adsorption mechanisms of ZCC nanomaterials for F^- were proposed based on the above data analysis (Scheme 2): 1. Ion exchange has occurred. LDHs are generated through hydrothermal technology under alkaline conditions using Zn^{2+}, Co^{2+}, and Cr^{3+} nitrates. The layers of LDHs contain embedded NO_3^-. The introduction of Cr^{3+} results in the positive charge of LDHs nanosheets interacting with the negative charge at the edge of the nanosheets, leading to the formation of a honeycomb structure. When F^- is adsorbed by the material, smaller F^- with a smaller radius enter the interlayer of LDHs by ion exchange, leading to a reduction in surface pores and lattice distortion of the LDHs. This phenomenon can be obtained from SEM after adsorption (Fig. 14a-c) and XRD (Fig. 14d). 2. A robust electrostatic attraction exists between ZCC nanomaterials and F^-. Compared to Zn-LDHs and Zn-Co-LDHs, the addition of more positively charged $M^{2+/3+}$ has a greater positive effect. This enhances intermolecular forces and increases the attraction between the positive charge on the surface of LDHs and F^-, resulting in increased adsorption between ZCC and F^-. Successive addition of Co^{2+} and Cr^{3+} increases the positive charge of Zn-LDHs, enhancing their electron attraction ability (Li et al.2022). This, in turn, promotes the absorption of F^- (Liu et al.,2023). 3. There is a van der Waals force between materials and ions.

4. Summary

In this paper, Zn-LDHs, Zn-Co-LDHs, Zn-Cr-LDHs, Co-Cr-LDHs, ZCC-1, ZCC-2 and ZCC-3 were prepared by hydrothermal method for the removal of F^- from water, and the results showed that the removal rate of ZCC-1, ZCC-2 and ZCC-3 increased significantly from 27.507 %, 30.437 % to 97.259 % after the addition of Cr modulation. ZCC-1, ZCC-2 and ZCC-3 adsorbents showed high removal rates for low concentration F^- solutions and the removal rates of F^- were higher than 90 % at different temperatures, dosing amounts, reaction times and pH. The maximum adsorption amounts of the materials were 108.87 mg/g, 97.27 mg/g and 97.62 mg/g, respectively. The adsorption of the three materials for F^- adsorption conformed to the quasi-secondary kinetic model and the Elovich model, and the isothermal adsorption data followed the Langmuir adsorption isotherm model. The reaction was an exothermic process, ion-exchange adsorption controlled by chemisorption, and the interaction of adsorption and desorption processes did not affect this adsorption kinetic process, and the calculated theoretical maximum adsorption amount was close to the actual maximum adsorption amount.

Author contribution Tian Huiyuan**:** investigation, formal analysis, writing and editing, conduct experiment. Li Yang: conduct experiment. Xia Mengyan: conduct experiment. Cui Baoyu: conduct experiment. Liu Chang: conduct experiment. Du Xiuhong: conduct experiment. Wang Zehua: conduct experiment. Duan Xianying: supervision. Cui Jiehu: conceptualization, methodology, supervision, writing and editing, funding acquisition. All authors read and approved the final manuscript.

This work was supported by the National Natural Science Foundation of China (21771165), Provincial Key Technologies R & D Program of Henan (232102310395), Henan Provincial University Science and Technology Innovation Team (24IRTSTHN008) and the Key Program of the Henan universities and colleges (20B150031, 19A140018).

Declaration of competing interest

The authors declare that they have no known competing financial interests or personal relationships that could have appeared to influence the work reported in this paper.

Appendix A. Supplementary data

Supplementary data to this article can be found online at https://doi.org/10.1016/j.arabjc.2024.105645.

References

Ali, S., Thakur, S.K., Sarkar, A., et al., 2016. Worldwide contamination of water by fluoride[J]. Environ. Chem. Lett. 14 (3), 291–315.

An, X., Jimmy, C.Y., Wang, Y., et al., 2012. WO3 nanorods/graphene nanocomposites for high-efficiency visible-light-driven photocatalysis and NO2 gas sensing[J]. J. Mater. Chem. 22 (17), 8525–8531.

Ayoob, S., Gupta, A.K., 2006. Fluoride in drinking water: a review on the status and stress effects[J]. Crit. Rev. Environ. Sci. Technol. 36 (6), 433–487.

Bekele, B., Lundehøj, L., Jensen, N.D., et al., 2019. Sequestration of orthophosphate by Ca2Al-NO3 layered double hydroxide-Insight into reactivity and mechanism[J]. Appl. Clay Sci. 176, 49–57.

Berner, S., Araya, P., Govan, J., et al., 2018. Cu/Al and Cu/Cr based layered double hydroxide nanoparticles as adsorption materials for water treatment[J]. J. Ind. Eng. Chem. 59, 134–140.

Cai, J., Zhang, Y., Pan, B., et al., 2016. Efficient defluoridation of water using reusable nanocrystalline layered double hydroxides impregnated polystyrene anion exchanger[J]. Water Res. 102, 109–116.

Coyote-Jiménez, J.C., Zavala-Arce, R.E., Jiménez-Núñez, M.L., et al., 2021. LDH-MgAl-NO3- synthesis with the intervention of ethylenediamine intended for the removal of fluoride ions from aqueous solution[J]. MRS Adv. 6 (43), 985–988.

Dang, R., Ma, X.R., Zhao, Y.P., et al., 2023. Construction of 3D Ni2+-Al3+-LDH/γ-Fe2O3-Cd2+-Ni2+-Fe3+-LDH structures and multistage recycling treatment of dye and fluoride-containing wastewater[J]. Chem. Eng. J. 451, 138499.

Dong, X., Chen, H., Zhao, W., et al., 2007. Synthesis and magnetic properties of mesostructured γ-Fe2O3/carbon composites by a co-casting method[J]. Chem. Mater. 19 (14), 3484–3490.

El Hassani, K., Beakou, B.H., Kalnina, D., et al., 2017. Effect of morphological properties of layered double hydroxides on adsorption of azo dye Methyl Orange: a comparative study[J]. Appl. Clay Sci. 140, 124–131.

Gupta, S.S., Bhattacharyya, K.G., 2011. Kinetics of adsorption of metal ions on inorganic materials: a review[J]. Adv. Colloid Interface Sci. 162 (1–2), 39–58.

He, S., Zhao, Y., Wei, M., et al., 2012. Fabrication of hierarchical layered double hydroxide framework on aluminum foam as a structured adsorbent for water treatment[J]. Ind. Eng. Chem. Res. 51 (1), 285–291.

Hem, J.D., 1959. Study and interpretation of the chemical characteristics of natural water. [J].

Jie, Z., Yichen, J., Ping, L., et al., 2022. Rational construction and understanding the effect of metal cation substitution of three novel ternary Zn-Co-Ni-LDHs from 2D to 3D and its enhanced adsorption properties for MO[J]. Environ. Sci. Pollut. Res. 1–19.

Kang, D., Yu, X., Tong, S., et al., 2013. Performance and mechanism of Mg/Fe layered double hydroxides for fluoride and arsenate removal from aqueous solution[J]. Chem. Eng. J. 228, 731–740.

Kang, D., Yu, X., Ge, M., 2017. Morphology-dependent properties and adsorption performance of CeO2 for fluoride removal[J]. Chem. Eng. J. 330, 36–43.

Koilraj, P., Kannan, S., 2013. Aqueous fluoride removal using ZnCr layered double hydroxides and their polymeric composites: Batch and column studies[J]. Chem. Eng. J. 234, 406–415.

Kong, L., Tian, Y., Pang, Z., et al., 2020. Needle-like Mg-La bimetal oxide nanocomposites derived from periclase and lanthanum for cost-effective phosphate and fluoride removal: characterization, performance and mechanism[J]. Chem. Eng. J. 382, 122963.

Li, J., Cui, J., Zheng, B., et al., 2019. Characterization of straw-doped and calcined modified zeolites for adsorption of copper and zinc ions[J]. Applied Chemistry 48 (7), 1558–1562.

Li, P., Jiang, Y., Tian, H., et al., 2022b. Study on the adsorption performance of NiCo-LDHs on anionic dye wastewater[J]. Shandong Chemical Industry 51 (18), 209–212.

Li, K., Li, S., Li, Q., et al., 2022a. Design of a high-performance ternary LDHs containing Ni, Co and Mn for arsenate removal[J]. J. Hazard. Mater. 427, 127865.

Li, Z., Zhang, X., Kang, Y., et al., 2021. Interface engineering of Co-LDH@ MOF heterojunction in highly stable and efficient oxygen evolution reaction[J]. Adv. Sci. 8 (2), 2002631.

Lin, J., Zhang, Y., Zhang, Q., et al., 2021. Enhanced adsorption properties of organic ZnCr-LDH synthesized by soft template method for anionic dyes[J]. Environ. Sci. Pollut. Res. 28 (35), 48236–48252.

Liu, J., Ali, A., Su, J., et al., 2021. Simultaneous removal of calcium, fluoride, nickel, and nitrate using microbial induced calcium precipitation in a biological immobilization reactor[J]. J. Hazard. Mater. 416, 125776.

Liu, F., Wan, L., Wang, H., et al., 2023. Unexpected F-removal by Co2Al-LDHs: Performance and new insight[J]. Chem. Eng. J. 452, 139400.

Luo, H., Wang, B., Liu, T., et al., 2019. Hierarchical design of hollow Co-Ni LDH nanocages strung by MnO2 nanowire with enhanced pseudocapacitive properties[J]. Energy Storage Mater. 19, 370–378.

Ma, X.R., Wei, X.Y., Dang, R., et al., 2021. A simple, environmentally friendly synthesis of recyclable magnetic γ-Fe2O3/Cd2+-Ni2+-Fe3+-CO32- layered double hydroxides for the removal of fluoride and cadmium ions. adsorption capacity and the underlying mechanisms[J]. Appl. Clay Sci. 211, 106191.

Mallakpour, S., Hatami, M., 2017. Biosafe organic diacid intercalated LDH/PVC nanocomposites versus pure LDH and organic diacid intercalated LDH: synthesis, characterization and removal behaviour of Cd2+ from aqueous test solution[J]. Appl. Clay Sci. 149, 28–40.

Mandal, S., Tripathy, S., Padhi, T., et al., 2013. Removal efficiency of fluoride by novel Mg-Cr-Cl layered double hydroxide by batch process from water[J]. J. Environ. Sci. 25 (5), 993–1000.

Mullen, J., 2005. History of water fluoridation[J]. Br. Dent. J. 199 (7), 1–4.

Noor, S., Rashid, A., Javed, A., et al., 2022. Hydrogeological properties, sources provenance, and health risk exposure of fluoride in the groundwater of Batkhela, Pakistan[J]. Environ. Technol. Innov. 25, 102239.

özcan A S, Gök Ö, özcan A., 2009. Adsorption of lead (II) ions onto 8-hydroxy quinolineimmobilized bentonite[J]. J. Hazard. Mater. 161 (1), 499–509.

Sahoo, D.P., Patnaik, S., Rath, D., et al., 2018. Synergistic effects of plasmon induced Ag@ Ag3VO4/ZnCr LDH ternary heterostructures towards visible light responsive O2 evolution and phenol oxidation reactions[J]. Inorg. Chem. Front. 5 (4), 879–896.

Sahoo, D.P., Patnaik, S., Parida, K., 2019. Construction of a Z-scheme dictated WO3-X/Ag/ZnCr LDH synergistically visible light-induced photocatalyst towards tetracycline degradation and H2 evolution[J]. ACS Omega 4 (12), 14721–14741.

Shinde, R.B., Patil, A.S., Sadavar, S.V., et al., 2022. Polyoxotungstate intercalated self-assembled nanohybrids of Zn-Cr-LDH for room temperature Cl2 sensing[J]. Sens. Actuators B 352, 131046.

Singh, K., Lataye, D.H., Wasewar, K.L., et al., 2013. Removal of fluoride from aqueous solution: status and techniques[J]. Desalin. Water Treat. 51 (16–18), 3233–3247.

Susheela, A.K., 1999. Fluorosis management programme in India[J]. Curr. Sci. 77 (10), 1250–1256.

Tan, Y., Sun, Z., Meng, H., et al., 2019. Efficient and selective removal of congo red by mesoporous amino-modified MIL-101 (Cr) nanoadsorbents[J]. Powder Technol. 356, 162–169.

Wu, J.C., Chen, S.S., Yu, T.C., et al., 2021. Effective electrochemically controlled removal of fluoride ions using electrodeposited polyaniline-carbon nanotube composite electrodes[J]. Sep. Purif. Technol. 254, 117561.

Xia, L., Zhang, W., Che, J., et al., 2021. Stepwise removal and recovery of phosphate and fluoride from wastewater via pH-dependent precipitation: Thermodynamics, experiment and mechanism investigation[J]. J. Clean. Prod. 320, 128872.

Xu, W., Mertens, M., Kenis, T., et al., 2022. Can high temperature calcined Mg-Al layered double hydroxides (LDHs) fully rehydrate at room temperature in vapor or liquid condition?[J]. Mater. Chem. Phys. 127113.

Yang, Y., Xu, X., Li, W., et al., 2023. Multi-color materials NiMn LDH loaded on activated carbon as electrode for electrochemical performance investigation[J]. Appl. Surf. Sci. 611, 155562.

Zeng, B., Wang, Q., Mo, L., et al., 2022. Synthesis of Mg-Al LDH and its calcined form with natural materials for efficient Cr (VI) removal[J]. J. Environ. Chem. Eng. 10 (6), 108605.

Zhang, X., Li, Y., Yang, Z., et al., 2022a. Industrially-prepared carbon aerogel for excellent fluoride removal by membrane capacitive deionization from brackish groundwaters[J]. Sep. Purif. Technol. 297, 121510.

Zhang, Y., Shi, B., Ma, B., et al., 2022b. Removal of fluoride from waste acid using lanthanum chloride: Defluoridation behavior and reaction kinetics of recovery process[J]. Process Saf. Environ. Prot. 167, 322–331.

Zheng, M., Wang, J., Fu, D., et al., 2023. Anchored growth of highly dispersed LDHs nanosheets on expanded graphite for fluoride adsorption properties and mechanism [J]. J. Hazard. Mater. 442, 130068.

Zhu, J., 2022. Study on the adsorption/photocatalytic degradation of LDHs and their nanocomposites on dye wastewater[D]. Zhengzhou Institute of Aviation Industry Management.